VERSITA

OPTO-ELECTRONICS REVIEW **14**(4), 323–328

DOI: 10.2478/s11772-006-0044-7

General properties of lasing effect in chiral liquid crystals

S.P. PALTO*[1], N.M. SHTYKOV[1], B.A. UMANSKY[1], M.I. BARNIK[1], and L.M. BLINOV[1,2]

[1]Shubnikov Institute of Crystallography, 59 Leninsky Sq., 119333 Moscow, Russia
[2]LICRYL – INFM Research Unit of Cosenza, Physics Department, University of Calabria, 87036 Rende (CS), Italy

Numerical simulations and experimental studies of the lasing effect in chiral liquid crystals are presented. It is shown that ring-like light emission, which is often observed experimentally, is a true lasing effect. Lasing condition and different modes in thin liquid crystal layers are discussed.

Keywords: liquid crystals, optics, lasing.

1. Introduction

Lasing effect in liquid crystals (LC) with helical distribution of the director field is a well-known phenomenon since the very first observations [1]. However, the proper understanding some of its basic features has appeared much later, when the interest in lasing in LC systems has been renovated [2–11]. The current interpretation of the effect is based on the photonic band-gap concept [2]. In accordance with this approach, chiral liquid crystal (CLC) layers are treated as one-dimensional photonic crystals. The well-known spectral band of the selective reflection, which is due to the helical distribution of the LC director, is just equivalent to the photonic band. Because the density of photon states achieves maxima just at the spectral boundaries of the band, namely these spectral regions are treated as most favourable for appearance of the low-threshold lasing effect. The lasing inside the photonic band-gap is forbidden unless defects are introduced into CLC layers [4–7].

The lasing in CLCs is an attractive phenomenon for many reasons. For instance, the CLC elements do not need additional mirrors. They can be made in a form of polymer films [8,9]. The sensitivity of LCs to external factors such as temperature, electric and magnetic fields is a promising feature for creating different lasing sensors [10]. The low threshold of the effect in CLC allows for the cascade excitation of the lasing emission, when subsequent LC cell is pumped by lasing from the previous one [11].

Despite many properties of lasing in CLC are already clear, there are still many principal features, which are not investigated in details. For instance, the well-known ring structure of light emission appearing during the lasing is not well explained. Lasing condition and distribution of generated modes also need to be investigated. To some extent, these problems are addressed in this work.

*e-mail: palto@online.ru

Here, we present both numerical simulation and experimental data on the lasing effect in CLCs doped by luminescence dyes. Our simulation approach is based on solving the Maxwell equations for stratified anisotropic media using the 4×4 matrix approach proposed by Berreman [12]. However, in order to simulate the lasing effect we allow negative absorption coefficients for CLC media and search for singularity solutions corresponding to the lasing condition. In more details, this approach is described in Ref. 13, where the lasing condition for thin LC layers is formulated in a matrix form.

The experimental studies were made on CLC layers doped with Oxazine-17 dye. With pulse pumping at 532 nm, oxazine dyes are suitable for the lasing effect in spectral region 590–650 nm. Spectral distribution of the lasing modes for normal and oblique directions, as well as their dependence on the LC amplification coefficients are discussed.

2. Lasing condition in thin LC layers

In order to clarify the lasing in case of thin LC layers, we repeat here some basics formulated in Ref. 13 by considering the simplest example of the optical problem for an isotropic and homogeneous plate **B** shown in Fig. 1. Let the plate has the thickness d, while the size in the xy directions is not limited. We are interested in propagation of a probe plane wave coming from the isotropic nonabsorbing media **A**. In a general case, the electromagnetic field in the plate **B** is just a superposition of eigen waves propagating in the forward and backward directions. Let at input point "1", the incident (source) wave is characterized by the Maxwell column $\vec{E} = (E_{s0}E_{p0})^T$, where the index p is attributed to the wave polarized in the plane of incidence, and s-index is for the orthogonal polarization. At boundary "12", this wave is partially transmitted into the plate and gives a contribution to the forward wave. This contribution at point

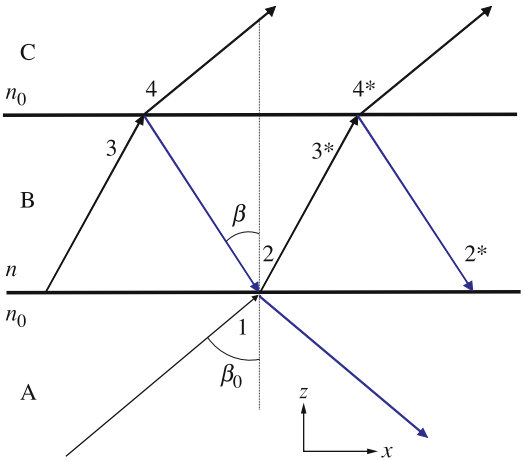

Fig. 1. A scheme of a LC layer represented by a Fabry-Perot plate (B) and propagating plane waves.

"2" (Fig. 1) can be designated as $\vec{E}_{21} = \mathbf{T}_{21}\vec{E}$, where $\mathbf{T}_{21}$ is the transmission matrix for "12" border. Here, the subscripts are related to designation of particular points. For instance, a subscript "21" means propagation from point "1" to point "2". Another contribution $\mathbf{R}_{21}\mathbf{P}_{23}\mathbf{R}_{34}\vec{E}_3$ to the forward wave at point "2" comes from the backward wave in the **B**-media. This contribution is a result of wave reflection at point "3", propagation to point "2" and, finally, reflection from boundary "21". Thus, as it is seen from Fig. 1, the resultant forward wave at point "2" is

$$\vec{E}_2 = \mathbf{T}_{21}\vec{E} + \mathbf{R}_{21}\mathbf{P}_{23}\mathbf{R}_{34}\vec{E}_3, \qquad (1)$$

where $\mathbf{R}_{34}$ is the reflection matrix for border "34", $\mathbf{P}_{23}$ is the wave propagating matrix from point "3" to point "2", $\mathbf{R}_{21}$ is the reflection matrix for border "21" and $\vec{E}_3$ is the field of the eigen forward wave at point "3". Because the plate is homogeneous in the x and y directions, the magnitude of the field of the forward wave at point "3" is equal to the magnitude at point "3*". The waves at "3" and "3*" are only shifted in phase by the value of $\delta_{33^*} = k_{0x}(x_3 - x_{3^*})$, so

$$\vec{E}_3 = \vec{E}_{3^*}\exp(-i\delta_{33^*}) = \mathbf{P}_{3^*2}\vec{E}_2\exp(-i\delta_{33^*}). \qquad (2)$$

Substituting Eq. (1) into Eq. (2) we get

$$\vec{E}_3 = \mathbf{P}_{3^*2}\exp(-i\delta_{33^*})(\mathbf{T}_{21}\vec{E} + \mathbf{R}_{21}\mathbf{P}_{23}\mathbf{R}_{34}\vec{E}_3). \qquad (3)$$

Then, as follows from Fig. 1, the field at the output is

$$\vec{E}_4 = \mathbf{T}_{43}\vec{E}_3. \qquad (4)$$

It is evident that Eqs. (3) and (4) can be represented by a circuit shown in Fig. 2. From Eqs. (3) and (4), we can explicitly express the field at output point "4" in the media **C** as

$$\vec{E}_4 = \mathbf{T}_{43}\vec{E}_3 = T_{43}(\mathbf{I} - \mathbf{P}_{3^*2}\mathbf{R}_{21}\mathbf{P}_{23}\mathbf{R}_{34}\exp(-i\delta_{33^*}))^{-1} \times \mathbf{P}_{3^*2}\mathbf{T}_{21}\vec{E}\exp(-i\delta_{33^*}), \qquad (5)$$

where **I** is the unity matrix.

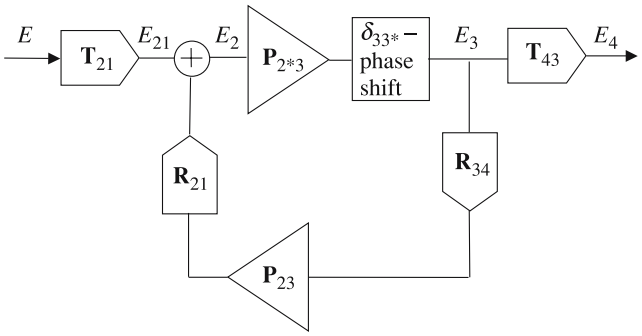

Fig. 2. Equivalent circuit which mimics performance of the Fabry-Perot plate.

Due to the feedback shown by the circuit in Fig. 2, Eq. (5) describes the solution of the optical problem on account of multiple reflections. From the linear circuit in Fig. 2, it is evident that in case of $\mathbf{P}_{3^*2}$ and $\mathbf{P}_{23}$ representing amplifiers this circuit can be a generator. The feedback coefficient is defined by the product $\mathbf{R}_{21}\mathbf{P}_{23}\mathbf{R}_{34}$, and the generation condition is

$$\det(\mathbf{F}) \equiv \det(\mathbf{P}_{3^*2}\mathbf{R}_{21}\mathbf{P}_{23}\mathbf{R}_{34}\exp(-i\delta_{33^*}) - \mathbf{I}) = 0. \qquad (6)$$

It is obvious that, in the case of the matrices replaced by scalars, Eq. (6) is just equivalent to the well-known condition for the oscillator circuit known in radio-engineering that is to unity of amplification coefficient over the round trip. From the mathematical point of view, Eq. (6) is the condition for singularity of matrix **F**. According to Eq. (5), if Eq. (6) is satisfied then any small fluctuation at the input results in infinite response at the output. It should be underlined that for the lasing Eq. (6) must be satisfied explicitly, any deviation of amplification from that defined by Eq. (6) results in suppression of generation.

So far, we have made no assumptions on properties of the **B** plate except its homogeneity in the x and y directions. The general properties of Eq. (6) remain valid also for anisotropic LC layers and in some particular cases the proper matrices can be found analytically [13]. The most principal consequence of the developed approach is that, for numerical simulation of the lasing effect in LCs, one needs to find singularity solutions of the optical problem. To do this, we have adapted the well-known Berreman matrix method [12].

Hence, complex multilayer systems including CLC layers can be simulated for the lasing effect. Another important consequence of this theoretical background is that in the case of thin layers, when the excitation (pumping) region is much larger than a layer thickness, the lasing condition can be satisfied in the whole range of angular directions. The latter can result in appearance of very pronounced ring-like structure, which is not just super-luminance, but true lasing effect.

3. Experimental results and numerical simulations

We made the simulations for CLC layer with the parameters very close to those measured for an experimental cell. Figure 3 shows the experimental and simulated spectra for a CLC layer (the ordinate values correspond to –log(T), where T is the transmission coefficient). Curve 1 in Fig. 3 is for the CLC material doped by 0.09% wt of the Oxazin-17 luminescent dye. In the CLC, this dye is characterized by maximum absorption at a wavelength of 540 nm that is well suited for optical pumping by a second harmonic of a Nd^{3+} YAG laser at 532 nm. The luminescence band of Oxazin-17 is located in a range of 560–650 nm with a maximum at 600 nm. In order to make a CLC with a photonic band in a spectral range of 578–618 nm (see curve 2 in Fig. 3), we have used a nematic LC matrix with the refractive indices $n_\perp$ = 1.487 and $n_\parallel$ = 1.595 (at T = 22°C) doped by 20% wt of optically active D-Leucine derivative. Curve 3 in Fig. 3 shows simulated spectrum for a CLC with the helix pitch P = 387.4 nm and refractive indices equal to those of the LC matrix. During this simulation no fitting parameters were used. Some disagreement between measured and simulated spectra can be attributed to changes of the refractive indices of LC after its doping by the chiral D-Leucine. Indeed, a width of the calculated photonic band gap is of about 5 nm wider compared to the experimentally measured value. At the same spectral locations (597 nm) of the centres of the calculated and measured selective reflection bands, the long-wave edge of the calculated band is located at a wavelength of 617 nm, while the corresponding experimental value is 611 ±1 nm. This wavelength difference points out the decrease in the optical anisotropy Δn of the LC mixture after doping the LC matrix by both the chiral D-Leucine derivative and the dye. We also underline that the mentioned spectral shift of about 5 nm is present in simulated data of lasing modes. This must be taken into ac-

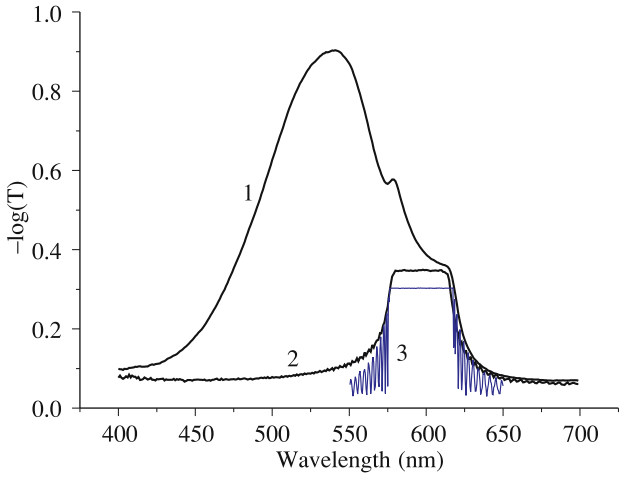

Fig. 3. Spectra of –log(T) (T is the transmission coefficient) for CLC layers: 1 – CLC is doped by Oxazin-17 dye, 2 – CLC layer without dye doping, and 3 – numerically simulated spectrum of the non-doped CLC.

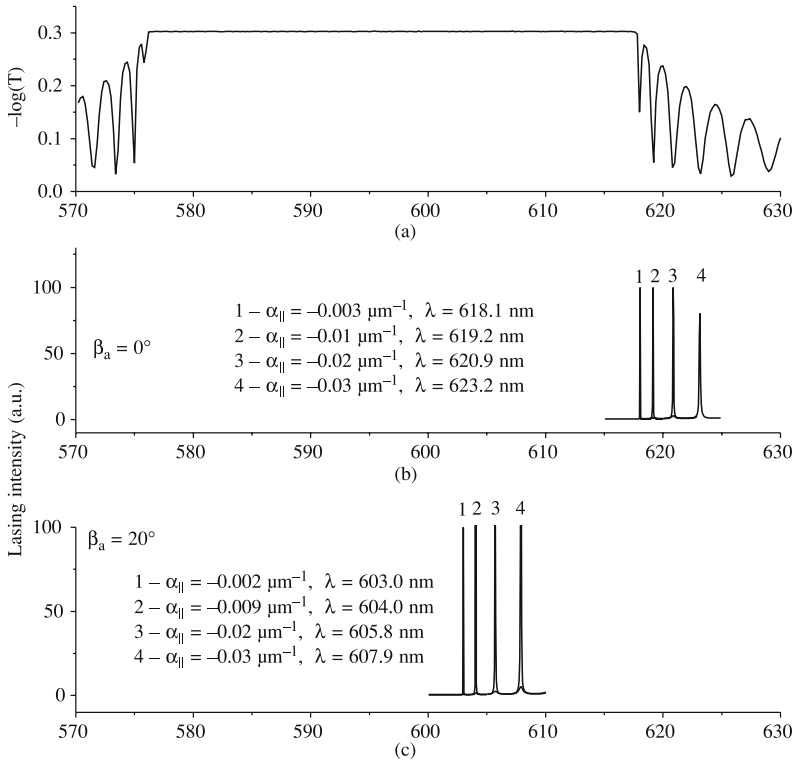

Fig. 4. Numerically simulated spectra: (a) –log(T) spectrum at normal incidence and zero absorption coefficient, (b) lasing effect along the normal direction in cases of different negative absorption $\alpha_\parallel$ satisfying the lasing condition, (c) lasing effect at an angle of 20° with respect to the normal for different absorption $\alpha_\parallel$ satisfying the lasing condition.

count when the experimental data are compared with the simulated results (see below). Imperfect LC alignment results in additional light scattering, which together with dye absorption raise the background experimental value of $-\log(T)$ compared to the calculated value, Fig. 3.

The results of simulation of the lasing effect are shown in Fig. 4. In our simulation, we consider the CLC layer placed between glass substrates with a refractive index of 1.5. The thickness of CLC is 30 μm that is close to a value for our experimental samples. We also assume that upon the optical pumping, the whole LC media is characterized by the negative absorption coefficient α or by the amplification coefficient $-\alpha$. Independent measurements of the luminescence spectra for Oxazin-17 in LC matrix show the positive dichroism, which allows us to assume that in the optically inverted LC media the value of the amplification $-\alpha_{\|}$ along the local LC director is higher than that $-\alpha_{\perp}$ for the perpendicular direction. Thus, during simulations, we were looking for singularity (lasing) solutions by varying the negative $\alpha_{\|}$ at $\alpha_{\perp} = 0$. In this situation, the lasing condition can be satisfied only at a long-wave boundary of the photonic band [Fig. 4(a)]. Figure 4(b) illustrates appearance of the singularities (lasing modes) for the direction parallel to the helical CLC axis. We remind that each of the lasing modes is available only for a unique value of the amplification $-\alpha_{\|}$. The list of the corresponding values is shown in within the figures. For instance lasing mode "1" at $\lambda = 618.1$ nm shown in Fig. 4(b) needs the lowest amplification of $-\alpha_{\|} = 0.003$ μm^{-1}, while the other modes appear at a higher amplification and, consequently, they are characterized by a higher extent of the excited states inversion. In the figure, we show only 4 modes. Actually, by increasing the amplification, one can excite more modes, which are located at lower frequencies. It is of crucial significance that the lasing condition can also be satisfied for the oblique directions. For instance, in Fig. 4(c) some of the lasing modes are shown propagating in air at the angle β_a of 20° with respect to the normal (inside the glass substrates with a refraction index $n_0 \cong 1.5$, the corresponding angle β_0 is approximately equal to 13°). Thus, the ring structure (Fig. 5) often observed experimentally is just the lasing effect. The left-side mode at $\lambda = 603$ nm is characterized by amplification coefficient $-\alpha_{\|} = 0.002$ μm^{-1}, which is even lower than in case of the lasing in the normal direction. The oblique modes are strong channels for energy leakage, which significantly reduces the efficiency of the lasing along the normal. The energy of the oblique modes is distributed over the whole angular sector that results in low energy density, especially for the modes characterized by low amplification. The latter makes some problems for direct measurements of these oblique lasing modes.

Figure 6 shows our experimental results on lasing. At normal direction [Fig. 6(b)], the lasing appears at a wavelength of 611 nm, which is indeed close to the long-wave photonic band boundary [Fig. 6(a)], but is still shifted by a few nanometers to the short waves. We assume that this

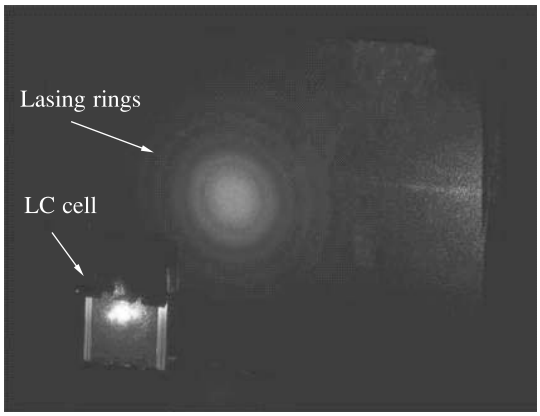

Fig. 5. Photo demonstrating the ring-type lasing in a CLC layer.

small shift is basically due to different conditions the lasing and transmission spectra were measured. The measured lasing wavelength $\lambda = 611.0$ nm is of about 7 nm shorter than a simulated wavelength of 618.1 nm, Fig. 4(b). This difference is well explained by the long-wave spectral shift of the photonic band in case of simulation as it was discussed above.

We were also capable to measure the emission spectra at an angle of 21° with respect to the normal, Fig. 6(c) that corresponds to a small part of energy distributed over the whole ring area of the emitted light. In order to increase the intensity of light inside the rings and measure the spectrum, we had to increase the pump energy 3 times in comparison with the pump necessary for observation of the normal lasing (we also checked that the lasing along the normal still exists at the wavelength of $\lambda = 611.0$ nm). The narrow spectral width of the emitted light indeed proves the lasing effect along this oblique direction. As it is predicted by numerical simulations, the wavelength of oblique "ring-type" lasing is shifted to the higher frequencies. In this particular case, the shift is ~1.9 nm. This spectral shift is too small to be associated with the oblique lasing mode of the lowest threshold. According to numerical simulations at an angle of 20°, the mode of the lowest threshold should be located at a wavelength of about 603 nm, while the measured wavelength is 609.1 nm. Moreover, if we take into account the mentioned systematic long-wave spectral shift (~5 nm) of the simulated photonic band edge then the numerical discrepancy becomes significant between the measured wavelength and wavelength of the simulated mode excited at the lowest amplification [$\alpha = 0.002$ μm^{-1}, curve 1 in Fig. 4(c)]. The experimental result is explained by simulations if we assume a higher amplification coefficient of the CLC mixture in the given direction than is necessary for the lowest threshold mode. For higher amplification, as follows from the simulations [see curves 2, 3, 4 in Fig. 4(c)], the modes at longer wavelengths can be excited. In order to simulate the lasing at a wavelength close to the measured one, we need to have the amplification higher than 0.03 μm^{-1}.

Thus, we have not observed the oblique lasing modes of the lowest threshold. Probably this is due to by their low in-

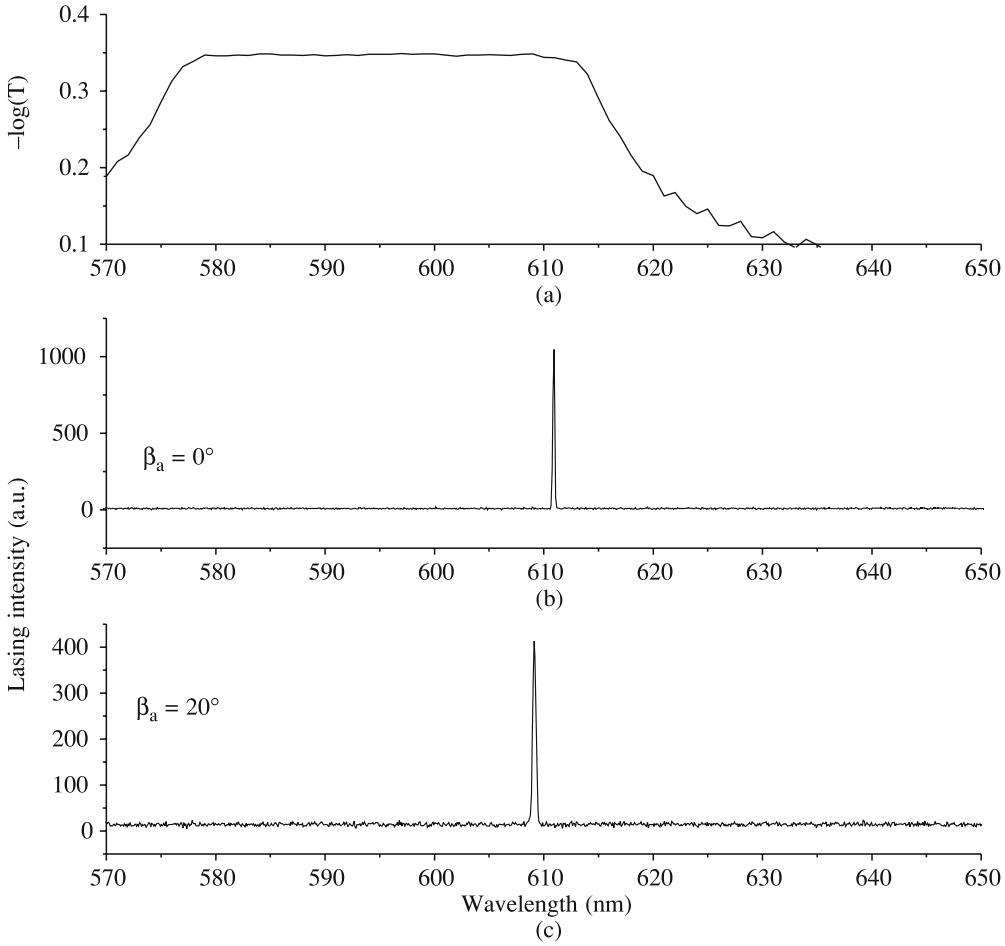

Fig. 6. Experimental spectra in CLC layer: (a) spectrum of the photonic band measured in CLC layer without luminescent dye, (b) lasing spectrum in dye-doped CLC layer measured along the normal direction (pump pulse energy is 4.5 μJ), and (c) lasing spectrum in dye-doped CLC layer measured at angle of 21° with respect to the normal direction (pump pulse energy is 11.6 μJ).

tensity that is a consequence of both low amplification coefficient and angular ("ring-like") energy distribution. Unfortunately, at current stage of study we do not know the properties of the excited states for the Oxazine-17 dye. Thus, we are not able to predict the spectral and angular dependence of the amplification coefficient on the pump intensity. Nevertheless, it is important that the experimental data do prove the most principal result following from the simulations – the rings can do represent a true lasing effect rather than a super-luminescence or diffraction divergence of the normal modes.

Figure 7 shows the data on the lasing intensity measured along the normal direction. These results allow estimating a pumping threshold value to be of about 4 μJ. On account of size of the pumping spot, the threshold intensity is estimated to be of about 5 mJ/cm^2. This value is rather high and we believe that one of the drawbacks resulting in the high threshold and lowering lasing intensity along the normal direction is related to energy leakage into the oblique "ring-type" lasing modes. In limit of angles approaching a value of $\pi/2$, with respect to the normal, the in-plane leaky modes can also be excited [13,14].

4. Conclusions

Using the lasing condition in case of the prolongated LC layers we have formulated basic approach for numerical simulation of the lasing effect. According to this approach,

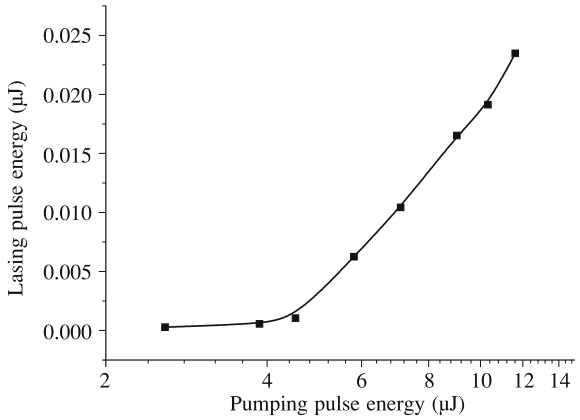

Fig. 7. Dependence of the lasing pulse energy (arbitrary units) on pump pulse energy at 533 nm. The estimated area of the pumping spot is of about 0.1 mm^2. The lasing energy is integrated over all directions with a cone angle of 9° with respect to the normal.

the lasing can be studied by searching singularity solutions of the optical problem on account of a negative absorption coefficient of LC media. Thus, the matrix methods, which have been developed for anisotropic stratified media can be efficiently used for these purposes. It is shown that in case of thin LC layers, the lasing is allowed in a wide range of angular directions. This property is proved by both numerical simulations and direct measurements. In a particular case of the cholesteric LC layers, the lasing condition can be satisfied for a large angular sector providing ring-type distribution of the light emission. This ring-type emission is a serious factor, which limits efficiency of CLC lasing elements.

Acknowledgments

The work is made in a frame of Russian Federal Project No 02.434.11.2025.

References

1. I.P. Il'chishin, E.A. Tikhonov, V.G. Tishchenko, and M.T. Shpak, "Generation of tunable radiation by impurity cholesteric liquid crystals", *JETP Lett*. **32**, 24 (1980).
2. V.I. Kopp, B. Fan, H.K.M. Vithana, and A.Z. Genack, "Low-threshold lasing at the edge of a photonic stop band in cholesteric liquid crystals", *Opt. Lett*. **23**, 1707 (1998).
3. B. Taheri, A.F. Munoz, P. Palffy-Muhoray, and R. Twieg, "Low threshold lasing in cholesteric liquid crystals", *Mol. Cryst. Liq. Cryst*. **358**, 73 (2001).
4. Y.C. Yang, C.S. Kee, J.E. Kim, H.Y. Park, J.C. Lee, and Y.J. Jeon, "Photonic defect modes of cholesteric liquid crystals", *Phys. Rev*. **E60**, 6852 (1999).
5. M. Becchi, S. Ponti, J.A. Reyes, and C. Oldano, "Defect modes in helical photonic crystals: An analytical approach", *Phys. Rev*. **B70**, 033103 (2004).
6. A. Matsui, M. Ozaki, and K. Yoshino, "Tunable photonic defect modes in a cholesteric liquid crystal induced by optical deformation of helix", *Phys. Rev*. **E69**, 061715 (2004).
7. V.I. Kopp, Z.Q. Zhang, and A.Z. Genack, "Lasing in chiral photonic structures", *Prog. Quant. Electron*. **27**, 369 (2003).
8. A.Y. Bobrovsky, N.I. Boiko, V.P. Shibaev, and J.H. Wendorff, "Cholesteric mixtures with photochemically tunable, circularly polarized fluorescence", *Adv. Mater.* **15**, 282 (2003).
9. T. Matsui, R. Ozaki, K. Funamoto, M. Ozaki, and K. Yoshino, "Flexible lasers made from cholesteric liquid crystal polymers", *Mol. Cryst. Liq. Cryst*. **413**, 2643 (2004).
10. M.F. Moreira, I.C.S. Carvalho, W. Cao, C. Bailey, B. Taheri, and P. Palffy-Muhoray, "Cholesteric liquid-crystal laser as an optic fiber-based temperature sensor", *Appl. Phys. Lett*. **85**, 2691 (2004).
11. A. Chanishvili, G. Chilaya, G. Petriashvili, R. Barberi, R. Bartolino, G. Cipparrone, and A. Mazzulla, "Laser emission from a dye-doped cholesteric liquid crystal pumped by another cholesteric liquid crystal laser", *Appl. Phys. Lett*. **85**, 3378 (2004).
12. D.W. Berreman, "Optics in stratified and anisotropic media: 4×4-matrix formulation", *J. Opt. Soc. Am*. **62**, 502 (1972).
13. S.P. Palto, "Lasing in liquid crystal thin films", *JETP* **103**, 469 (2006).
14. L.M. Blinov, G. Cipparrone, P. Pagluisi, V.V. Lazarev, and S.P. Palto, "Mirrorless lasing from nematic liquid crystals in the plane waveguide geometry without refractive index or gain modulation", *Appl. Phys. Lett*. **89**, 0311114 (2006).

